Photoluminescence of CdTe nanocrystals modulated by methylene blue and DNA. A label-free luminescent signaling nanohybrid platform

Jiang-Shan Shen,[a] Tao Yu,[ab] Jian-Wei Xie[b] and Yun-Bao Jiang*[a]

Received 7th January 2009, Accepted 11th March 2009
First published as an Advance Article on the web 26th March 2009
DOI: 10.1039/b900053d

A nanohybrid consisting of water-soluble thioglycolic acid (TGA)-capped CdTe nanocrystals (NCs) and methylene blue (MB) was designed as a label-free luminescent signaling platform for DNA. This sensing system was identified to operate under the photoinduced electron transfer (PET) mechanism in which MB is the electron acceptor and the binding site for the designated target molecule DNA. We showed that MB bound with TGA-capped CdTe NCs *via* strong electrostatic interactions resulted in an efficient quenching of the photoluminescence (PL) of NCs. Steady-state and time-resolved PL, and electron paramagnetic resonance (EPR) experiments established the quenching pathway of PET from the conduction band (CB) of NCs to the ground state of MB. In the presence of the target molecule DNA, the MB-quenched PL of NCs could be reversibly restored by double-stranded DNA as the PET pathway is blocked when MB is taken away from the NCs surface due to its intercalation into, and electrostatic interaction with, DNA. The platform was successfully applied for sensing DNA and signaling DNA hybridization by switching the PET process. Such a nanohybrid represents a robust PET luminescent nanosensor that is, in principle, applicable for other species by employing suitable electron acceptors as binding sites.

Introduction

II–VI semiconductor nanocrystals (NCs), especially cadmium chalcogenide NCs, have attracted widespread interest over the past decades due to substantial development of their synthetic methods and intriguing photophysical properties. II–VI semiconductor NCs are known for their photostability, high photoluminescence (PL) quantum yield, broad absorption spectrum with high molar extinction coefficient (10–100-fold that of organic dyes), and their symmetric, narrow and tunable emission spectrum spanning from UV to near IR. These properties make them attractive for numerous applications, ranging from light-emitting diodes to bioimaging, biolabeling and sensing, with performances that are significantly superior to their organic counterparts.[1–7] Although many smart fluorescent organic dyes have been intensively investigated for sensing a variety of target molecules, following mechanisms such as photoinduced electron transfer (PET) and energy transfer,[8,9] constructing II–VI semiconductor NC-based nanohybrids for recognition and sensing will be an important extension of NCs' applications. It is expected that NC-based sensing systems would overcome some of the shortcomings of traditional organic dye-based chemosensors, such as photobleaching, narrow excitation and untunable emission spectra.

Recently, there have been several reports on Förster fluorescence resonance energy transfer (FRET)-based bio-sensor design and protein conformation studies using inorganic II–VI semiconductor NC-luminophores as energy donors or acceptors.[5,10–21] Results suggested that FRET applications using NCs offered unique advantages over conventional organic dyes. These include the abilities of NCs in tuning the extent of spectral overlap with a given organic acceptor by size variation and providing a favorable configuration at which several donors or acceptors can be arrayed around a single NC's surface thereby affording enhanced FRET cross-section. Limitations, however, exist such as the large size of NC–bioreceptor conjugates that might lead to aggregation and the high cost of dye-labeled bioreceptors. Efficient strategies for constructing II–VI semiconductor NC-based nanohybrids remain to be explored to provide more stable and simpler recognition and sensing. NC-based hybrids consisting of an NC-luminophore and a small organic molecule bearing a binding site that has an electron/hole transfer channel are considered potential alternatives. Electron/hole transfer between II–VI semiconductor NCs and organic molecules attached to the NCs' surface have been extensively investigated for optoelectronic devices and solar cells.[22] The potential of such NC-based nanohybrids as PET nanobiosensors are promising, since modulation of this PET process by the target molecule may result in enhancement or quenching of the PL of NCs that affords an observable signal output. In fact, little effort has been made to this kind of NC's nanosensors for small molecules and biomolecules.[23–32] Moreover, most of the related investigations employed well-documented electron acceptors, such as viologens of

[a] *Department of Chemistry, College of Chemistry and Chemical Engineering, and the MOE Key Laboratory of Ananlytical Sciences, Xiamen University, Xiamen, 361005, China. E-mail: ybjiang@xmu.edu.cn; Fax: +86 (0)592-218-5662; Tel: +86 (0)592 218 5662*
[b] *Beijing Institute of Pharmacology and Toxicology, Beijing, 100850, China*

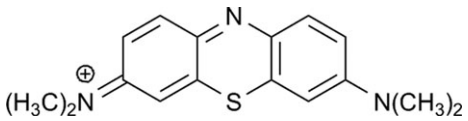

Scheme 1 Molecular structure of MB.

relatively high cytotoxicity,[33] just to demonstrate the occurrence of PET process. Thus, developing safe and feasible electron or hole acceptors remains a challenge and highly demanded for constructing NC-based nanosensors under electron/hole transfer mechanism.

Herein, we present a simple and facile strategy for constructing an II–VI semiconductor NC-based nanohybrid for PET luminescent signaling. In this module, methylene blue (MB, Scheme 1), a DNA intercalator and antimalarial drug,[34] are linked *via* electrostatic interactions to the surface of water soluble thioglycolic acid (TGA)-capped CdTe NCs. Electrostatic interaction between NCs and MB facilitates PET from excited NCs to MB, leading to quenching of PL of NCs. We showed that this nanohybrid indeed acted as a PET luminescent signaling platform for DNA and DNA hybridization. This is because that MB is released from the NCs' surface due to its intercalation into and electrostatic interactions with double stranded DNA, which blocks PET process and thereby restores PL of NCs, enabling a new and label-free DNA detection scheme. In principle, this strategy will offer an efficient means of creating new II–VI semiconductor NC-based nanobiosensors that are applicable to any other NCs that are linked to a suitable electron/hole acceptor bearing interaction sites for target species.

Experimental

Synthesis of NaHTe

NaHTe was obtained according to a previously reported method with minor modifications.[35] A mixture of 0.16 g tellurium powder and 0.2 g $NaBH_4$ was added into a 10 mL flask fitted with a pinhead and rubber tube that was connected to a water seal. The flask was deaerated by a continuous nitrogen flow, to which 3.0 mL of N_2-saturated H_2O was injected at 0 °C. After 6 h, the black Te powder completely disappeared and white sodium tetraborate precipitated. The resultant transparent supernatant solution was used as the Te precursor for the following procedures.

Synthesis of TGA-capped CdTe naocrystals

TGA modified CdTe NCs were synthesized by using $CdCl_2$ and NaHTe as precursors, following reported methods with minor changes.[35,36] 0.23 g $CdCl_2$ was dissolved in 100 mL Milli-Q water, to which 0.3 mL TGA was added. 0.1 M NaOH was added dropwise under vigorous stirring to adjust solution pH to 8. The solution gradually became optically transparent during this process. Deaeration of the solution was carried out under a flow of nitrogen with stirring at room temperature for *ca.* 30 min. Next, the freshly synthesized NaHTe solution was quickly injected into the mixture *via* a syringe with vigorous stirring. The molar ratio of Cd^{2+}:TGA:HTe^- was fixed at 1 : 3 : 0.5. The solution was then refluxed at 100 °C under nitrogen for various durations to obtain CdTe NCs of varied sizes. The CdTe NCs solution was exposed to room light for about a month, resulting in stabilized CdTe/CdS core–shell structure due to photodegradation of TGA.[37,38]

DNA hybridization

25 nmol C-DNA (capture DNA) and 25 nmol completely complementary DNA (P-DNA, perfect match) were respectively dissolved in a 1-mL vial using 50 μL pH 6.8 buffer solution containing 120 mM NaCl, 10 mM KCl, 5 mM $MgCl_2$, and 120 mM citric acid. Two solutions were then mixed and heated at 90 °C for 5 min. After cooling to room temperature, the solution was left stand for 50 min to complete the hybridization. Incubation of C-DNA and complete noncomplementary DNA (I-DNA, irrelevant) was similarly carried out. A certain amount of incubated DNA or calf thymus (ct) DNA was then added into NCs-MB buffer solutions for further spectral measurements.

Characterization

UV-visible absorption spectra were recorded on a Varian Cary 300 absorption spectrophotometer using a 1-cm quartz cell. The absorbance of NCs sample at the excitation wavelength (400 nm) was made lower than 0.05 in order to avoid self-absorption. PL spectra were taken on a Hitachi F-4500 fluorescence spectrophotometer using excitation and emission slits of 5 nm. Room-temperature PL quantum yields (Q_D) were determined using quinine sulfate as a standard (0.546 in 0.5 M H_2SO_4[39]). High resolution transmission electron microscopy (HRTEM) experiments were carried out on Tecnai F30 300 KV. X-Ray diffractions (XRD) were performed on Panalytical X'pert PRO diffractometer equipped with Cu Kα radiation (λ = 1.5418 Å) under room temperature. Electron paramagnetic resonance (EPR) was measured using a Bruker EMX-10/12 spectrometer. PL decay curves were measured on a Horiba JobinYvon FL3-TCSPC system. Cyclic voltammetry experiments of MB were performed in 10 mM Tris–HCl buffer of pH 7.4 containing 100 mM KCl as supporting electrolyte. A conventional three-electrode cell was employed which was equipped with Pt plates as working and counter electrode and saturated calomel electrode as a reference electrode. Scan rate was 50 mV s^{-1} and the solution was deoxygenated by N_2 for at least 30 min prior to the measurements.

Results and discussion

Fig. 1 shows that TGA-capped CdTe NCs have a well-resolved exciton absorption peak at 515 nm that corresponds to the lowest energy excitonic transition of 2.4 eV. This indicates a good monodispersity of the prepared NCs in 10 mM Tris–HCl buffer of pH 7.4. Particle size was calculated to be 2.8 nm, from the exciton absorption maximum using an empirical formula given by Peng *et al.*[40] for particles synthesized *via* an organometallic route. This was supported by HRTEM images (Fig. 2) which show that TGA-capped CdTe NCs are crystals, sufficiently monodisperse and well separated, with a narrow size distribution around a mean value of 3.4 nm. The emission spectrum demonstrates a

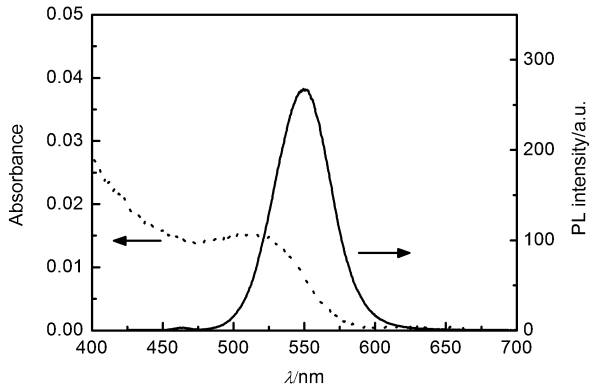

Fig. 1 UV-vis absorption (dashed) and PL (solid) spectra of TGA-capped CdTe NCs in 10 mM Tris-HCl buffer of pH 7.4. [NCs] = 1.73×10^{-7} M, λ_{ex} = 400 nm.

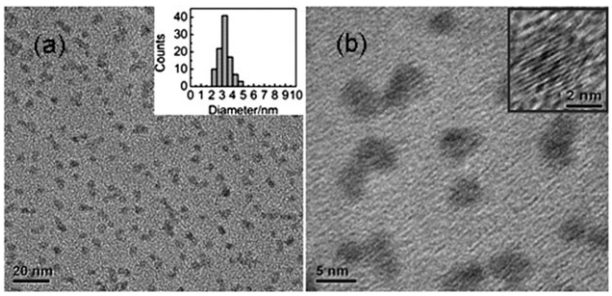

Fig. 2 Representative HRTEM images of TGA-capped CdTe NCs. Scale bar is 20 nm (a), 5 nm (b), and 2 nm (inset in b), respectively. Inset in (a) is size distribution of TGA-capped CdTe NCs from HRTEM images.

symmetric and sharp band with a maximum of 550 nm that is close to its absorption onset (Fig. 1), indicating that the emission is due to direct recombination of conduction and valence band charge carriers.[38] Powder XRD pattern of TGA-capped CdTe NCs is given in Fig. 3, from which typical peaks for NCs due to quantum size effect of nanocrystals are observed. The nanocrystals were indicated as a cubic (zinc blende) structure that is also the dominant crystal phase of bulk CdTe. The diffraction pattern of TGA-capped CdTe NCs after room light exposure moved slightly towards higher angles, suggesting the formation of CdS shell on CdTe,[37] but could not indicate the integrality of the shell. The mean particle size can be alternatively calculated by the well-known Scherrer equation,

$$D = 0.89\ \lambda/(\beta \cos \theta) \quad (1)$$

in which D is the diameter of nanocrystals, λ is the wavelength of the incident X-ray, β is full width at half-maximum, and θ is diffraction angle. The average particle size of TGA-capped CdTe NCs thus estimated is 2.6 nm, consistent with that from HRTEM and that calculated from the Peng formula.[40]

Concentration of NCs could be estimated for further using *via* the extinction coefficient that was also obtained from the result of Peng *et al.*[40] To assess the possibility of using water-soluble TGA-capped CdTe NCs in chemo/biosensing, photo-stability of NCs in 10 mM Tris-HCl aqueous buffer of pH 7.4 was examined. The PL signal was found to be hardly changed after 1 h, indicating that the NCs are stable in the tested buffer, similar to that reported by Eychmüller *et al.*[41]

In the presence of MB, a significant and regular decrease in the PL intensity of TGA-capped CdTe NCs was observed. This was accompanied by a slight blue shift of the emission maximum (Fig. 4a). Stern–Völmer quenching constant was calculated to be as 1.03×10^6 M^{-1} at low MB concentration (Fig. 4b). Such a high value indicates that MB is strongly associated to the surface of NCs by electrostatic interactions. Evidences for the formation of CdTe NCs–MB complexes came also from ionic strength dependence of quenching of PL intensity of NCs that it became less prominent with increasing ionic strength (Fig. 5). Influence of NCs on absorption spectra of MB was monitored. Fig. 6 shows that, with increasing concentration of CdTe NCs, absorbance of MB at 664 nm decreases together with the development of the absorption at 520 nm and a crosspoint at 565 nm. Benesi–Hildebrand analysis[43] of the absorption data afforded an apparent association constant K_{app} of 3.72×10^6 M^{-1}, which corresponds to a free energy change ΔG of -37.5 kJ mol^{-1} at 298 K. These data further illustrate the strong affinity of MB towards CdTe NC's surface.

Several mechanisms for the quenching by MB of PL of NCs can be considered: (i) energy transfer from smaller to bigger

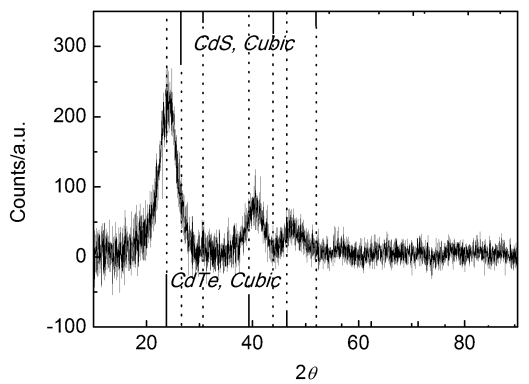

Fig. 3 XRD pattern of TGA-capped CdTe NCs. The line spectra correspond to standard diffraction lines for cubic phase of bulk CdTe and CdS, respectively.[37,42]

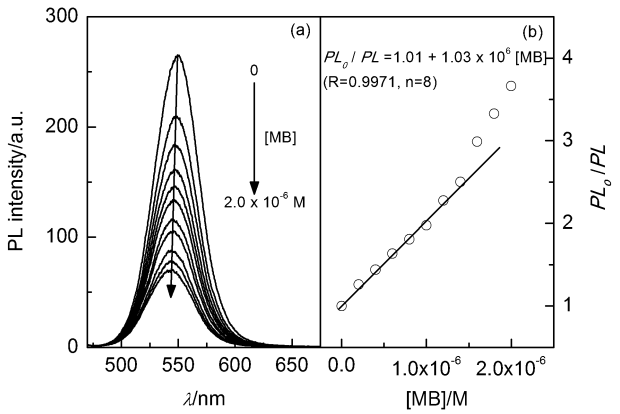

Fig. 4 PL spectra of TGA-capped CdTe NCs in the presence of MB (a) and Stern–Völmer plot (b) in 10 mM Tris–HCl buffer of pH 7.4. [NCs] = 1.73×10^{-7} M, λ_{ex} = 400 nm.

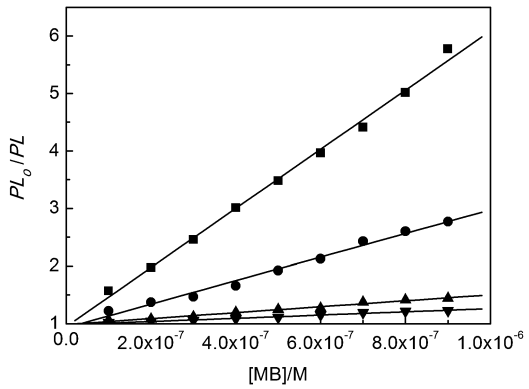

Fig. 5 Stern–Völmer plots for quenching PL of TGA-capped CdTe NCs by MB in the presence of NaCl. [NaCl] = 0 mM (■), 10 mM (●), 50 mM (▲), 100 mM (▼). [NCs] = 1.73×10^{-7} M, [MB] = 0–9.0×10^{-7} M, λ_{ex} = 400 nm.

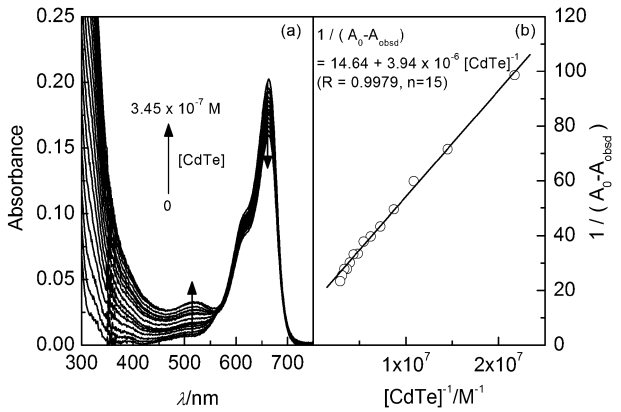

Fig. 6 (a) Absorption spectra of MB in the presence of TGA-capped CdTe NCs and (b) double reciprocal plot of $1/(A_0 - A_{obsd})$ *versus* 1/[CdTe] in 10 mM Tris-HCl buffer of pH 7.4. [NCs] = 0–3.45×10^{-7} M, [MB] = 2.0×10^{-6} M.

NCs; (ii) FRET from NCs to MB; and (iii) electron or hole transfer from excited NCs to MB. The first possibility was taken into consideration since NCs solution in general contains NCs of varied sizes despite the observed narrow size distribution in the present case (Fig. 2). The absorption spectra of larger NCs overlap heavily with the emission spectra of smaller NCs due to the quantum confinement effect, excitation energy of a smaller NC could therefore be transferred to a larger NC as a result of the proximity or aggregation of the particles.[44] The reported most pronounced effect of NC-aggregation is a bathochromic shift in emission. The fact that a slight blue shift was observed upon quenching by MB of the PL of NCs (Fig. 4a) however indicates that the quenching is not due to NC-aggregation. This is also supported from the HRTEM investigations which show that NC particles are similarly dispersed in the absence and presence of MB under spectral measurment concentrations.

On the basis of Förster formalism, there are at least three requirements for FRET to occur from NCs to MB, *i.e.* efficient overlap between PL spectrum of NCs and absorption spectrum of MB, center-to-center distance of NCs and MB, and coupling between NCs and MB transition dipole

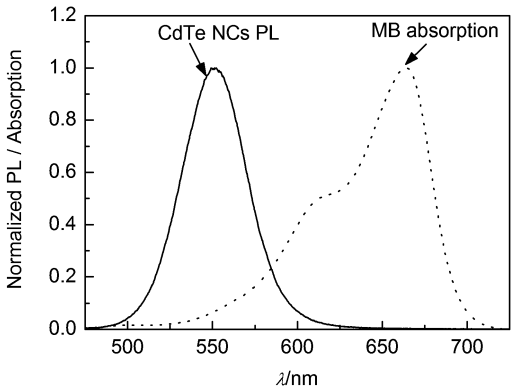

Fig. 7 Normalized PL spectrum of TGA-capped CdTe NCs and absorption spectrum (ε_A) of MB.

moments. Spectra presented in Fig. 7 indicate that the absorption of MB and PL of NCs PL do overlap despite not very much. The overlap integral $J(\lambda)$ and Förster radius R_0 were calculated according to the following equations,[45]

$$J(\lambda) = \int_0^\infty PL_D(\lambda)\, \varepsilon_A(\lambda)\, \lambda^4\, d\lambda \quad (2)$$

$$R_0^6 = 8.79 \times 10^{-5} [k^2\, n^{-4} Q_D J(\lambda)] \quad (3)$$

in which PL_D and ε_A represent normalized NCs PL spectrum and MB absorption spectrum (expressed in extinction coefficient), respectively; $k^2 = 2/3$ for randomly oriented dipoles; n is refractive index of the medium, $n = 1.33$ for water; and Q_D is PL quantum yield of NCs, $Q_D = 0.027$.

The overlap integral and Förster radius thus calculated were 5.13×10^{11} M^{-1} cm^{-1} nm^4 and 7.98 Å, respectively. The space length of TGA molecule in the NC–MB complexes was calculated to be 7 Å by using Gaussian 03W package,[46] which was then used to deduce the center-to-center distance r between NCs and MB of *ca.* 24 Å using a NC radius of *ca.* 17 Å from HRTEM images. The energy transfer efficiency was therefore calculated from the following formula,[5]

$$E = mR_0^6/(mR_0^6 + r^6) \quad (4)$$

in which m is the average number of acceptor molecules interacting with one NC particle. A value of m lower than 10 was estimated on the basis of MB to NCs concentration ratio, leading to an energy transfer efficiency of lower than 0.0133. This means that the energy transfer from NCs to MB is negligible.

The observed quenching therefore likely originated from an electron or a hole transfer process. Fig. 8 depicts the energy level positions of conduction (CB) and valence (VB) band edges of TGA-capped CdTe NCs and the HOMO and LUMO of MB (detailed calculations given in the Appendix). In principle, electron or hole trapping from excited NCs to an electron or a hole acceptor attached to NC's surface, respectively, is energetically possible if the LUMO energy level of the electron acceptor is below the CB energy level of NCs or the HOMO energy level of the hole acceptor is above the VB energy level of NCs. E_{HOMO} of −6.26 eV and E_{LUMO} of −4.55 eV *vs.* vac of MB and E_{CB} of −2.96 eV and E_{VB} of −5.36 eV *vs.* vac of NCs were obtained and shown in Fig. 8. Therefore, electron transfer from CB of excited NCs to MB is

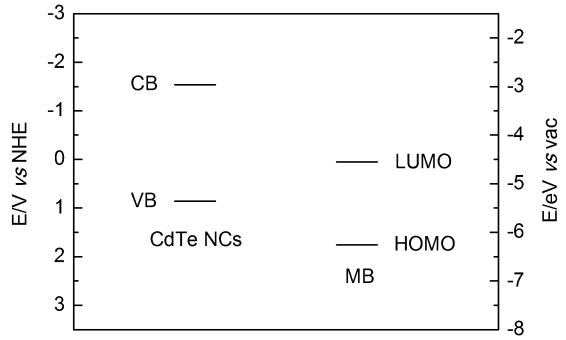

Fig. 8 Energy level diagram showing positions of CB and VB edges of TGA-capped CdTe NCs and the HOMO and LUMO of MB measured in 10 mM Tris-HCl buffer of pH 7.4.

energetically favorable, yet hole transfer from VB of excited NCs to MB is energetically forbidden. This electron transfer process was further proven by the following data. For radiative recombination both hole and electron are needed. Thus, when the electron is trapped to a MB molecule, a competition between electron trapping and radiative recombination occurs. This would lead to a decrease in the PL of NCs with increasing MB concentration, as what was experimentally observed. Efficient PET process is likely responsible for the blue shift observed in the PL spectra of NCs in the presence of MB.[47,48]

Electron paramagnetic resonance (EPR) was employed to confirm the occurrence of electron transfer process. A clear signal of the NC–MB complex with a *g*-tensor of 2.0048 and a linewidth ΔH_{app} of 14 G was observed after illumination under $\lambda < 400$ nm (Fig. 9b). This EPR signal was assigned to the MB radical resulting from electron transfer from the excited NCs to the bound MB molecules. Control experiments with NCs or MB alone (Fig. 9a,c) showing no EPR signal supported this conclusion.

Time-resolved PL experiments using time correlated single photon counting (TCSPC) technique were carried out to analyze the electron transfer process from excited CdTe NCs to MB. Fig. 10 shows that the decay of TGA-capped CdTe NCs is multi-exponential with decay time components (τ_i) of varied pre-exponential factors (α_i), 3.41 ns (10.89%), 20.72 ns (69.69%), and 89.55 ns (19.42%). This multi-exponential

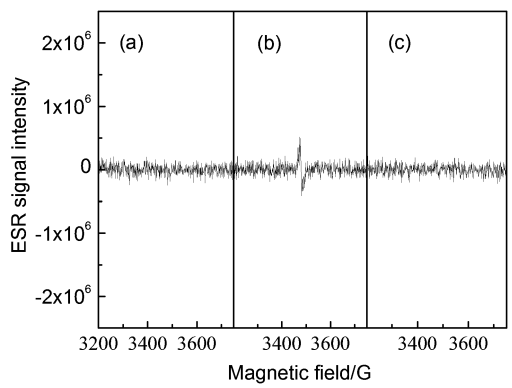

Fig. 9 X-Band differential EPR spectra measured after UV illumination of TGA-capped CdTe NCs in the absence (a) and presence (b) of MB. Spectrum (c) is that measured after illumination of MB alone. Frequency is 9.763 GHz; UV lamp, $\lambda < 400$ nm, 300 W.

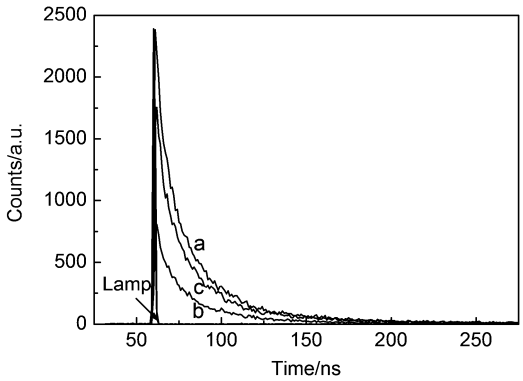

Fig. 10 PL decay curves of CdTe NCs in the absence (a) and presence (b) of MB. (c) is PL decay curve of CdTe NCs in the presence of MB and ct DNA in 10 mM Tris-HCl buffer of pH 7.4. $\lambda_{ex} = 380$ nm, $\lambda_{em} = 550$ nm, [CdTe NCs] = 1.73×10^{-7} M, [MB] = 2.0×10^{-6} M, [ct DNA] = 5.0×10^{-5} M.

decay behavior is characteristic of PL dynamics of II-VI NCs due to complicated nonradiative pathways involving probably trapping electron or hole by defects on NCs surface[49,50] and blinking effects.[51,52] The shortest decay time of 3.41 ns observed in this investigation is in agreement with that of previous report[38] and with that obtained theoretically of *ca.* 3 ns.[53] The decay times of NCs in the presence of MB of 1.79 ns (7.61%), 16.72 ns (59.71%), and 49.07 ns (32.68%), are distinctly shorter. The calculated average decay time of NCs in the presence of MB is therefore shorter (Table 1). Nonradiative (k_{nr}) and radiative (k_r) rate constants could be calculated using the following equations,[45]

$$Q_D = k_r/(k_r + k_{nr}) \quad (5)$$

$$\tau = 1/(k_r + k_{nr}) \quad (6)$$

$$k_r = Q_D/\tau \quad (7)$$

Data compiled in Table 1 indeed point out increased nonradiative rate constant and suppressed radiation transition of NCs in the presence of MB. This is again in line with the occurrence of electron transfer from CdTe NCs to MB.

PL of NCs partially quenched by MB was found to recover upon addition of calf thymus (ct) DNA, accompanied by a bathochromic shift (Fig. 11). Indeed, cationic MB, one of the most popular biological probes, has been shown to interact with double stranded DNA mainly *via* intercalation and insertion into both the minor and major grooves of the double helix.[54] Theoretical calculations and experiments suggested a stronger tendency of intercalation of MB into GC than AT base sequences in the MB–DNA complexes.[54,55] MB bound to

Table 1 Average PL decay time ($\langle\tau\rangle$), quantum yield (Q_D), radiative (k_r) and nonradiative (k_{nr}) rate constants

Sample	$\langle\tau\rangle^a$, ns	Q_D	k_r, s^{-1}	k_{nr}, s^{-1}
CdTe	57.69	0.027	4.68×10^5	1.68×10^7
CdTe–MB	36.48	0.009	2.47×10^5	2.72×10^7
CdTe–MB–ct DNA	46.14	0.019	4.12×10^5	2.13×10^7

[a] $\langle\tau\rangle$ represents average PL decay time calculated by $\langle\tau\rangle = \Sigma\alpha_i\tau_i^2/\Sigma\alpha_i\tau_i$, in which α_i is pre-exponential factor and τ_i is individual decay time.[45]

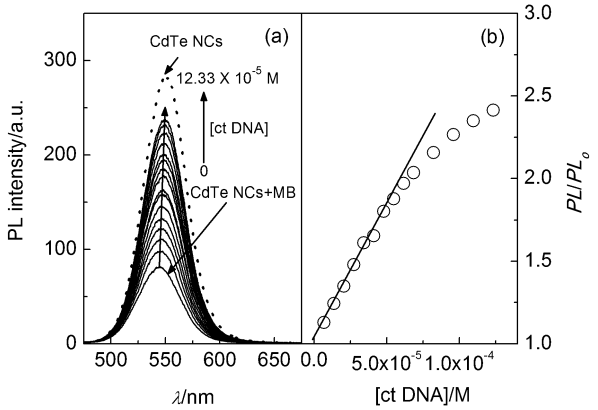

Fig. 11 (a) PL of TGA-capped CdTe NCs in 10 mM pH 7.4 Tris-HCl buffer upon addition of MB and ct DNA and (b) ct DNA response plot obtained from (a). [NCs] = 1.73×10^{-7} M, [MB] = 2.0×10^{-6} M, [ct DNA] = 0–12.33×10^{-5} M, λ_{ex} = 400 nm.

ct DNA would result in MB's release from NCs surface and hence block the electron transfer from excited NCs to MB, restoring PL of NCs.

A linear relationship was found between NCs PL intensity and ct DNA concentration at low ct DNA concentration (Fig. 11b). The restoration of NCs PL was found depending on the incubation time of ct DNA with NCs-MB nanohybrid that 5 min was needed to reach the maximum emission. In agreement with PL restoration, a longer decay time was detected and a higher radiative rate constant calculated in the presence of ct DNA (Fig. 10 and Table 1). The PL enhancement offers a robust platform for label-free DNA sensing system bearing both the unique properties of NC-luminophore and the merits of well-established PET mechanism.

To explore the potential of this nanohybrid platform in DNA hybridization sensing, single stranded DNA (capture DNA, C-DNA) with a sequence of 5′-CTGACTTCCATTGTC-3′, its complete complementary DNA with a sequence of 5′-GACAATGGAAGTCAG-3′ (perfect match DNA, P-DNA) and a complete noncomplementary DNA with a sequence of 5′-TTTCCGTATGCCTTA-3′ (irrelevant DNA, I-DNA) were designed. Fig. 12 shows that the double stranded DNA (ds-DNA) formed by hybridization of C-DNA and P-DNA enables restoration of PL of NCs previously quenched by MB, and the recovery depends on ds-DNA concentration. A linear correlation of $PL/PL_0 = 1.16 + 7.99 \times 10^5$ [ds-DNA] ($r = 0.9967$) was found over ds-DNA concentration of 1.25×10^{-7} to 1.25×10^{-6} M. The relative standard deviation was determined to be 1.13% with a detection limit (3s/k, $n = 11$) of 4.23×10^{-8} M for ds-DNA.

Under the same conditions, PL restoration of NCs by C-DNA, P-DNA, I-DNA, and C-DNA plus I-DNA were found all to be lower than that of ds-DNA (Fig. 12b), suggesting that the interaction of MB with single DNA (ss-DNA, such as C-DNA, P-DNA, and I-DNA) is only of electrostatic nature differing from that of ds-DNA. This distinct difference in PL restoration allows for a selective sensing of DNA. In the absence of MB, however, a negligible change in the PL spectra of the NCs was observed by the same amount of DNA, ruling out the formation of NCs-DNA complexes, likely due to electrostatic repulsions.

A scheme of "ON–OFF–ON" switching in the PL signal of the nanohybrid for DNA sensing is presented in Scheme 2. It illustrates that TGA-capped CdTe NCs interact efficiently with MB that results in PL quenching, leading to an "OFF" state. In the presence of DNA, intercalation and/or electrostatic interaction between MB and DNA releases MB from NCs surface and hence restore the PL from NCs, recovering the "ON" state again.

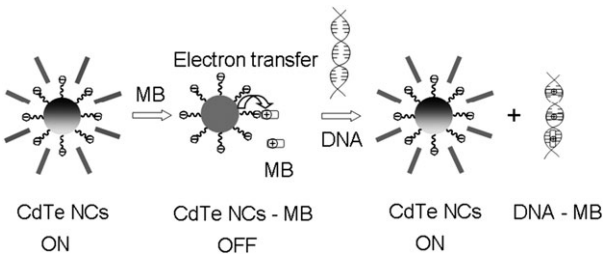

Scheme 2 Schematic diagram of DNA sensing.

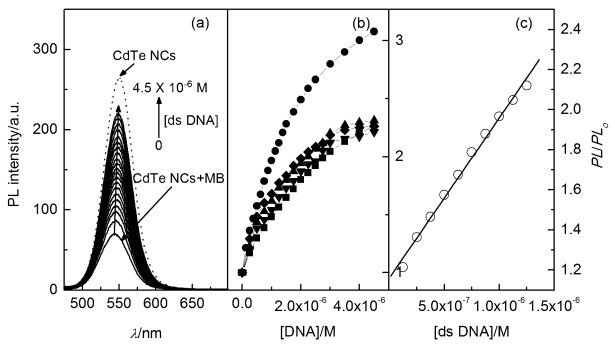

Fig. 12 (a) PL spectra of TGA-capped CdTe NCs in 10 mM pH 7.4 Tris-HCl buffer upon addition of MB and ds-DNA of increasing concentration, (b) response plots of (●) ds-DNA, (■) C-DNA, (▼) P-DNA, (◆) I-DNA, and (▲) C-DNA and I-DNA, and (c) linear response plot of ds-DNA at low concentration. [NCs] = 1.73×10^{-7} M, [MB] = 2.0×10^{-6} M, λ_{ex} = 400 nm.

Conclusions

TGA-capped CdTe NCs were synthesized in aqueous solutions and characterized. NCs were used to construct a nanohybrid system with MB *via* electrostatic interactions. Such a nanohybrid shows much weaker PL compared to that of NCs. Electron transfer from excited NCs to MB was identified to quench the PL of NCs, on the basis of steady-state and time-resolved PL and electron paramagnetic resonance (EPR) data. PL of NCs could be restored by double stranded DNA (ds-DNA) by inhibiting this electron transfer process *via* taking MB away through intercalation into and electrostatic interactions with the DNA strands. Single stranded DNA (ss-DNA) could also restore the PL of this nanohybrid but to a lower extent since only electrostatic interaction exists between MB and ss-DNA. Incubation of capture DNA and its complete noncomplementary DNA was found to bring about PL restoration to an extent similar to

that of ss-DNA. This distinct difference thus allows for a selective sensing of ds-DNA and ss-DNA and for signaling DNA hybridization. Although several II–VI semiconductor NC-based signaling platforms for DNA sensing have been reported,[19,21,56,57] our system shows merits of being simple, label-free and low cost. The nanohybrid strategy presented here is expected to be of general applicability, subject to a suitable choice of an electron acceptor, for II–VI semiconductor NCs and for interaction with a diversity of target molecules. An electron acceptor that brings about stronger quenching of the PL of NCs, yet shows selective interactions with the target molecule, would be preferred.

Appendix

Calculations of potentials of conduction and valence bands of NCs

The conduction and valence band potentials of TGA-capped CdTe NCs are calculated using a simple effective mass calculation which weights the amount of the confinement energy given to the conduction and valence bands according to electron and hole effective masses,[58,59]

$$E_{CB}(NCs) = E_{CB}(bulk) + \Delta E_{conf} m_h (m_h + m_e)^{-1} \quad (A1)$$

$$\Delta E_{conf} = E_{1s}(NCs) - E_g(bulk) \quad (A2)$$

in which ΔE_{conf} is total confinement energy, E_{1s}(NCs) is the lowest energy excitonic transition of NCs, E_g(bulk) is bulk band gap of CdTe (1.56 eV *vs.* vac was chosen for the value of E_g),[60] and m_h and m_e are hole and electron effective masses of CdTe ($m_h = 0.4\ m_0$, $m_e = 0.11\ m_0$), respectively.[60] Following parameters could then be obtained,

$$\Delta E_{conf} = E_{1s}(NCs) - E_g(bulk) = 0.84 \text{ eV}$$

$$m_h(m_h + m_e)^{-1} = 0.78$$

The potential of the conduction band of NCs depends also on solution pH according to Nernstian equation,

$$E_{CB}(pH) = E_{CB}(pH_0) - 2.303RT\ pH/F \quad (A3)$$

in which $E_{CB}(pH_0)$ is standard potential of conduction band of NCs, R, F and T are the gas constant, Faraday constant, and absolute temperature, respectively. A value of −0.5 V *vs.* NHE was chosen for the potential value of the condution band of bulk CdTe in aqueous solution at pH 1.[22,61] E_{CB} of the bulk CdTe at pH 7.4 was hence calculated as −0.88 V *vs.* NHE.

To convert from V to eV, following equation was employed,

$$E(V) = e\text{NE(eV)}/nF \quad (A4)$$

in which e is an elemental charge, n is number of electrons exchanged in the reaction, N is Avogadro's constant and F is Faraday constant. In case of one electron reaction the numerical value of free energy in eV is equal to numerical value of the redox potentials in V. Thus,

$$E_{CB}(bulk) = -0.88 \text{ eV } (vs \text{ NHE, pH} = 7.4)$$

And to convert from the NHE scale to the vac scale, following formula was used,

$$E\ (vs \text{ NHE}) = -4.5 - E\ (vs \text{ vac}) \quad (A5)$$

Therefore, E_{CB} (bulk) = −3.62 eV (*vs* vac, pH = 7.4).

Further, according to A1, in vacuum,

$$E_{CB}\ (NCs) = E_{CB}(bulk) + \Delta E_{conf} m_h\ (m_h + m_e)^{-1} = -2.96 \text{ eV}$$

$$E_{VB}\ (NCs) = E_{CB}(NCs) - E_{1s}(NCs) = -5.36 \text{ eV}$$

Then,

$$E_{CB}\ (NCs) = -1.54 \text{ V } (vs \text{ NHE, pH} = 7.4)$$

$$E_{VB}\ (NCs) = 0.86 \text{ V } (vs \text{ NHE, pH} = 7.4)$$

Calculations of LUMO and HOMO energy levels of MB

The energy level of LUMO of MB could be estimated according to the following equation,

$$E_{LUMO}\ (vs \text{ vac}) = -4.5 - E'_{red}\ (vs \text{ NHE}) \quad (A6)$$

in which E'_{red} is the reduction potential onset of MB. A value of −195 mV *vs.* SCE was chosen for E'_{red}, from the cyclic voltammogram of MB (corresponding 46.5 mV *vs.* NHE).

Hence, E_{LUMO} = −4.55 eV (*vs* vac).

The HOMO–LUMO energy gap of 1.71 eV of MB was estimated from the absorption edge in term of transmittance.[62] Thus, E_{HOMO} (*vs* vac) of −6.26 eV was obtained from the equation of $E_g = E_{LUMO} - E_{HOMO}$.

Acknowledgements

We greatly appreciate the support of the National Natural Science Foundation of China (grants 20425518, 20675069, and 20835005). Thanks are due to Prof. Dr Shu-Lin Zhao and Prof. Dr Jian-Niao Tian of Guangxi Normal University for their generous helps in time-resolved PL experiments.

References

1 W. C. W. Chan and S. Nie, *Science*, 1998, **281**, 2016.
2 M. Bruchez Jr, M. Moronne, P. Gin, S. Weiss and A. P. Alivisatos, *Science*, 1998, **281**, 2013.
3 M. Han, X. Gao, J. Z. Su and S. Nie, *Nat. Biotechnol.*, 2001, **19**, 631.
4 I. L. Medintz, H. T. Uyeda, E. R. Goldman and H. Mattoussi, *Nat. Mater.*, 2005, **4**, 435.
5 A. R. Clapp, I. L. Medintz, J. M. Mauro, B. R. Fisher, M. G. Bawendi and H. Mattoussi, *J. Am. Chem. Soc.*, 2004, **126**, 301.
6 B. P. Aryal and D. E. Benson, *J. Am. Chem. Soc.*, 2006, **128**, 15986.
7 Y. Chen and Z. Rosenzweig, *Anal. Chem.*, 2002, **74**, 5132.
8 P. D. Beer and P. A. Gale, *Angew. Chem., Int. Ed.*, 2001, **40**, 486.
9 T. W. Bell and N. M. Hext, *Chem. Soc. Rev.*, 2004, **33**, 589.
10 E. R. Goldman, E. D. Balighian, H. Mattoussi, M. K. Kuno, J. M. Mauro, P. T. Tran and G. P. Anderson, *J. Am. Chem. Soc.*, 2002, **124**, 6378.
11 I. L. Medintz, A. R. Clapp, J. S. Melinger, J. R. Deschamps and H. Mattoussi, *Adv. Mater.*, 2005, **17**, 2450.
12 E. Oh, M.-Y. Hong, D. Lee, S.-H. Nam, H. C. Yoon and H.-S. Kim, *J. Am. Chem. Soc.*, 2005, **127**, 3270.
13 A. R. Clapp, I. L. Medintz, B. R. Fisher, G. P. Anderson and H. Mattoussi, *J. Am. Chem. Soc.*, 2005, **127**, 1242.
14 P. T. Snee, R. C. Somers, G. Nair, J. P. Zimmer, M. G. Bawendi and D. G. Nocera, *J. Am. Chem. Soc.*, 2006, **128**, 13320.

15 C.-Y. Chen, C.-T. Cheng, C.-W. Lai, P.-W. Wu, K.-C. Wu, P.-T. Chou, Y.-H. Chou and H.-T. Chiu, *Chem. Commun.*, 2006, 263.
16 M. Tomasulo, I. Yildiz and F. M. Raymo, *J. Phys. Chem. B*, 2006, **110**, 3853.
17 L. Shi, V. D. Paoli, N. Rosenzweig and Z. Rosenzweig, *J. Am. Chem. Soc.*, 2006, **128**, 10378.
18 L. Shi, N. Rosenzweig and Z. Rosenzweig, *Anal. Chem.*, 2007, **79**, 208.
19 H. Peng, L. Zhang, T. H. M. Kjällman, C. Soeller and J. Travas-Sejdic, *J. Am. Chem. Soc.*, 2007, **129**, 3048.
20 B. Tang, L. Cao, K. Xu, L. Zhuo, J. Ge, Q. Li and L. Yu, *Chem.–Eur. J.*, 2008, **14**, 3637.
21 R. Gill, I. Willner, I. Shweky and U. Banin, *J. Phys. Chem. B*, 2005, **109**, 23715.
22 A. Hagfeldt and M. Grätzel, *Chem. Rev.*, 1995, **95**, 49.
23 D. B. Cordes, S. Gamsey and B. Singaram, *Angew. Chem., Int. Ed.*, 2006, **45**, 3829.
24 I. Yildiz, M. Tomasulo and F. M. Raymo, *Proc. Natl. Acad. Sci. U. S. A.*, 2006, **103**, 11457.
25 J. H. Choi, K. H. Chen and M. S. Strano, *J. Am. Chem. Soc.*, 2006, **128**, 15584.
26 R. Gill, R. Freeman, J.-P. Xu, I. Willner, S. Winograd, I. Shweky and U. Banin, *J. Am. Chem. Soc.*, 2006, **128**, 15376.
27 S. J. Clarke, C. A. Hollmann, Z. Zhang, D. Suffern, S. E. Bradforth, N. M. Dimitrijevic, W. G. Minarik and J. L. Nadeau, *Nat. Mater.*, 2006, **5**, 409.
28 M. Tomasulo, I. Yildiz, S. L. Kaanumalle and F. M. Raymo, *Langmuir*, 2006, **22**, 10284.
29 V. Maurel, M. Laferrière, P. Billone, R. Godin and J. C. Scaiano, *J. Phys. Chem. B*, 2006, **110**, 16353.
30 F. M. Raymo and I. Yildiz, *Phys. Chem. Chem. Phys.*, 2007, **9**, 2036.
31 W. Chen, X. Wang, X. Tu, D. Pei, Y. Zhao and X. Guo, *Small*, 2008, **4**, 759.
32 J. Yuan, W. Guo, X. Yang and E. Wang, *Anal. Chem.*, 2009, **81**, 362.
33 D. G. Soares, A. C. Andreazza and M. Salvador, *J. Agric. Food Chem.*, 2003, **51**, 1077.
34 F. Gut, W. Schiek, W. E. Haefeli, I. Walter-Sack and J. Burhenne, *Eur. J. Pharm. Biopharm.*, 2008, **69**, 582.
35 H. Zhang, Z. Zhou, B. Yang and M. Gao, *J. Phys. Chem. B*, 2003, **107**, 8.
36 H. He, H. Qian, C. Dong, K. Wang and J. Ren, *Angew. Chem., Int. Ed.*, 2006, **45**, 7588.
37 H. Bao, Y. Gong, Z. Li and M. Gao, *Chem. Mater.*, 2004, **16**, 3853.
38 S. J. Byrne, S. A. Corr, T. Y. Rakovich, Y. K. Gun'ko, Y. P. Rakovich, J. F. Donegan, S. Mitchell and Y. Volkov, *J. Mater. Chem.*, 2006, **16**, 2896.
39 J. N. Demas and G. A. Croby, *J. Phys. Chem.*, 1971, **75**, 991.
40 W. W. Yu, L. Qu, W. Guo and X. Peng, *Chem. Mater.*, 2003, **15**, 2854.
41 K. Boldt, O. T. Bruns, N. Gaponik and A. Eychmüller, *J. Phys. Chem. B*, 2006, **110**, 1959.
42 A. L. Rogach, T. Franzl, T. A. Klar, J. Feldmann, N. Gaponik, V. Lesnyak, A. Shavel, A. Eychmüller, Y. P. Rakovich and J. F. Donegan, *J. Phys. Chem. C*, 2007, **111**, 14628.
43 P. V. Kamat, *J. Phys. Chem.*, 1989, **93**, 859.
44 R. Wargnier, A. V. Baranov, V. G. Maslov, V. Stsiapura, M. Artemyev, M. Pluot, A. Sukhanova and I. Nabiev, *Nano Lett.*, 2004, **4**, 451.
45 B. Valeur, *Molecular Fluorescence (Principles and Applications)*, Wiley-VCH Publishers, 2002.
46 M. J. Frisch, G. W. Trucks, H. B. Schlegel, G. E. Scuseria, M. A. Robb, J. R. Cheeseman, V. G. Zakrzewski, J. A. Montgomery, Jr., R. E. Stratmann, J. C. Burant, S. Dapprich, J. M. Millam, A. D. Daniels, K. N. Kudin, M. C. Strain, O. Farkas, J. Tomasi, V. Barone, M. Cossi, R. Cammi, B. Mennucci, C. Pomelli, C. Adamo, S. Clifford, J. Ochterski, G. A. Petersson, P. Y. Ayala, Q. Cui, K. Morokuma, P. Salvador, J. J. Dannenberg, D. K. Malick, A. D. Rabuck, K. Raghavachari, J. B. Foresman, J. Cioslowski, J. V. Ortiz, A. G. Baboul, B. B. Stefanov, G. Liu, A. Liashenko, P. Piskorz, I. Komaromi, R. Gomperts, R. L. Martin, D. J. Fox, T. Keith, M. A. Al-Laham, C. Y. Peng, A. Nanayakkara, M. Challacombe, P. M. W. Gill, B. G. Johnson, W. Chen, M. W. Wong, J. L. Andres, C. Gonzalez, M. Head-Gordon, E. S. Replogle and J. A. Pople, *GAUSSIAN 03 (Revision A.1)*, Gaussian, Inc., Pittsburgh, PA, 2003.
47 D. M. Guldi, G. M. A. Rahman, V. Sgobba, N. A. Kotov, D. Bonifazi and M. Prato, *J. Am. Chem. Soc.*, 2006, **128**, 2315.
48 D. M. Guldi, I. Zilbermann, G. Anderson, N. A. Kotov, N. Tagmatarchis and M. Prato, *J. Am. Chem. Soc.*, 2004, **126**, 14340.
49 N. Chestnoy, T. D. Harris, R. Hull and L. E. Brus, *J. Phys. Chem.*, 1986, **90**, 3393.
50 C. Landes, C. Burda, M. Braun and M. A. EI-Sayed, *J. Phys. Chem. B*, 2001, **105**, 2981.
51 M. Nirmal and L. Brus, *Acc. Chem. Res.*, 1999, **32**, 407.
52 F. Koberling, A. Mews and T. Basché, *Adv. Mater.*, 2001, **13**, 672.
53 B. L. Wehrenberg, C. Wang and P. Guyot-Sionnest, *J. Phys. Chem. B*, 2002, **106**, 10634.
54 E. Tuite and B. Nordén, *J. Am. Chem. Soc.*, 1994, **116**, 7548.
55 R. Rohs, H. Sklenar, R. Lavery and B. Röder, *J. Am. Chem. Soc.*, 2000, **122**, 2860.
56 C.-L. Feng, X. Zhong, M. Steinhart, A.-M. Caminade, J.-P. Majoral and W. Knoll, *Adv. Mater.*, 2007, **19**, 1933.
57 D. Cui, B. Pan, H. Zhang, F. Gao, R. Wu, J. Wang, R. He and T. Asahi, *Anal. Chem.*, 2008, **80**, 7996.
58 J. L. Blackburn, D. C. Selmarten, R. J. Ellingson, M. Jones, O. Micic and A. J. Nozik, *J. Phys. Chem. B*, 2005, **109**, 2625.
59 M. Sykora, M. A. Petruska, J. Alstrum-Acevedo, I. Bezel, T. J. Meyer and V. I. Klimov, *J. Am. Chem. Soc.*, 2006, **128**, 9984.
60 S. V. Gaponenko, *The Characteristics of Optics of Semiconductors Nanometer Crystals*, Springer, 1998.
61 S. F. Wuister, C. d. M. Donegá and A. Meijerink, *J. Phys. Chem. B*, 2004, **108**, 17393.
62 Y. Tian, T. Newton, N. A. Kotov, D. M. Guldi and J. H. Fendler, *J. Phys. Chem.*, 1996, **100**, 8927.